https://doi.org/10.1016/j.apenergy.2021.117059

A novel three-dimensional wake model based on anisotropic Gaussian distribution for wind turbine wakes

Ruiyang He[a, *], Hongxing Yang[a, *], Haiying Sun[a], Xiaoxia Gao[b]

a Renewable Energy Research Group (RERG), Department of Building Services Engineering, The Hong Kong Polytechnic University, Hong Kong

b Department of Power Engineering, North China Electric Power University (Baoding), China

* Corresponding author

E-mail address: ruiyang.he@connect.polyu.hk; hong-xing.yang@polyu.edu.hk

Abstract

The development of a more advanced three-dimensional wake model for wind power generation is presented based on a multivariate Gaussian distribution. The newly-presented model is closer to reality as it truly depends on two independent dimensions (namely horizontal and vertical directions) rather than the radius of a circle. For this reason, the general expression of wake expansion rate in each dimension is specifically developed. In addition, by taking into account the inflow wind shear effect, this current model is able to accurately capture the asymmetric distribution of the vertical wake profile. Four cases including experimental data from wind tunnels and field observations as well as high-fidelity numerical simulation are used to validate the present model. Compared with conventional models, this new model is capable of predicting the wake distribution of a single wind turbine reasonably well. The proposed model is highly simple with a low computational cost. Before applying this model, no additional numerical calculation or trial calculation is required. Wake velocity at any given spatial position can be calculated in an accurate and fast manner. Because of its accuracy, universality and low cost, the present three-dimensional wake model is able to make contributions to farm-level applications such as layout optimization and control strategies and therefore benefit the power output of wind farms.

Keywords: *Three-dimensional wake model; Multivariate Gaussian distribution; Anisotropic wake expansion rate; Wind tunnel and field measurement validation*

1. Introduction

Renewable energy applications like wind [1] and solar energy system deployment [2], as well as thermal and electrical energy storages [3], can decrease the primary energy consumption, reduce carbon dioxide emission and realize the carbon-neutral community. As efforts continue to accelerate the transition to renewable energy [3] from the conventional energy consumption model worldwide [4], the Global Wind Energy Council 2019 declared that wind energy has enjoyed a globally rapid expansion from 2009 to date [5]. In the meantime, the global wind industry reaches its milestone with new annual installations surpassing 60GW for only the second time in history [6]. Despite the fast growth of wind energy in past decades, challenges remain. The most significant one is the wake loss in wind farms. The wake effect appears downstream of one or several operating wind turbines characterized by lower wind speed and higher turbulence intensity. Wake from upstream wind turbines can negatively affect the electricity output of downstream rows, resulting in wake loss typically accounted for 10-20% of the total power generation [7]. Also, underestimation or overestimation of the wake effect will both lead to an inaccurate prediction of energy yields, exerting pressure on the power grid and servo system. As challenges surface, methods to understand the wake effect and predict wake losses within a wind farm have been explored by many researchers.

Wake loss models can be categorized into analytical wake models and numerical wake models based on computational fluid dynamics (CFD). The CFD-based wake models solve either Reynolds-Averaged Navier-Stokes (RANS) equations [8] or large-eddy simulation (LES) [9] governing the entire flow field. The computational requirements from fast analytical models to RANS-based models to high-fidelity LES increase exponentially. Since one of the most important applications of the wake model is to identify potential wake loss and therefore optimize wind turbine layout from the perspective of the wind farm level, the heavy computational costs of the numerical wake model are not practically feasible.

By taking advantage of high computational efficiency, considerable accuracy, and simple form, analytical models are widely used in practice for predicting wake distribution [10] and

power generation [11]. Jensen model is the most famous analytical wake model proposed by Jensen in 1982 [12] and then refined by Katic [13]. This one-dimensional model assumes a linear wake expansion and a top-hat shape of wind speed distribution. Its simplicity and robustness in the calculation [14] lead to its long-term mainstream status. However, Jensen model ignores the turbulence effect of inflow and predicts a uniform wake distribution that depends only on the downstream distance. The Frandsen model [15] also retains the classic top-hat shape and therefore suffers from the same drawbacks. With the rapid development of the analytical wake model, it can be demonstrated that the top-hat shape distribution of wake deficit obviously contradicts with the realistic Gaussian distribution from the theoretical [16], numerical simulation [17], and experimental point of view [18,19].

The recent state-of-the-art analytical wake models are extensively based on the assumption that the wake velocity follows the Gaussian distribution. A two-dimensional (2D) Gaussian-shape wake model inspired by Jensen model was derived by Gao[20]. Ge et al. [21] developed the Gaussian wake model with a linear wake expansion rate and made an approximation of wake boundary based on LES and experimental data. The authors further proposed a wake model [22] following the mass conservation locally and globally to fix the problem that solving the Jensen model first would violate the local mass conservation.

In order to harvest more wind energy by a single wind turbine, the inflow speed variation along with the vertical direction corresponding to the swept area should be taken into account with the trend of higher hub height and wider rotors. Therefore, the development of a 3D wake model is meaningful and appealing. Among them, the wake model proposed by Bastankah and Porté-Agel [23], the BPA model hereafter, is widely used. The BPA model is derived by applying mass and momentum conservation law and assuming a self-similar Gaussian distribution for the velocity deficit. Compared with the 1D model mentioned before, the BPA model significantly improves the accuracy of wake flow prediction and therefore becomes a foundation of more advanced wake models [24,25]. Although this model explicitly contains three variables x, y and z respectively representing downstream, horizontal and vertical directions, the values of y and z are effectively dependent on each other through the distance to the central line. A 3D wake model was derived by Sun [26] and validated against wind tunnel measured data with good agreement. Later this model was extended to 3D multi-wind turbine wake model [27] and the field experiments [19] proved that its application on complex terrain is feasible. Ishihara et al. [28] corrected the divergence and inaccuracy of the near wake region in the BPA model and used self-similarity and Gaussian distribution to

determine the added turbulence intensity. Besides, Dou et al. [29] developed a 3D yawed wake model to figure out the optimal yaw angle misalignment to improve the electricity yields.

Almost all the researches before assume that the wake profiles obey the Gaussian axisymmetric distribution. In recent years, researches from Xie [17], Abkar and Porté-Agel [30] have shed light on the non-axisymmetric nature of wake deficit, especially the far-field wake deficit, because it has anisotropic expansion rates in the vertical and horizontal directions. Xie [17] found that wind shear and the effect of ground may attribute to the anisotropic distribution in the wake profile. Abkar and Porté-Agel [30] held that the above feature of wake is mainly related to the fact that ambient turbulence intensity is stronger in the horizontal direction than that in the vertical direction and verified it with LES results. The resulting higher momentum contributes to a higher mean kinetic energy entrainment in the horizontal direction, which shows an agreement with the meandering characteristics of wake. Inspired by the above observation, a 3D elliptical wake model was developed by Gao [31] and validated by the conducted field experiments. To describe anisotropic expansion in the wake, the same expression of the wake expansion rate is adopted in two directions with different ambient turbulence intensities in horizontal and vertical directions collected by the field experiments. However, the turbulence intensities in two directions are not always available in the open-source experimental parameters. By using a modified elliptical BPA model taking account of the anisotropic expansion of the wake, Xie [17] shows its ability to improve the underestimation of the original model in the far wake regions. The elliptical Gaussian wake model proposed by Abkar and Porté-Agel [30] was utilized to estimate the influence of atmospheric stability on wake distribution. The results show that the wake grows faster horizontally than vertically for all stability cases, in which the non-axisymmetry of the wake profile under convective conditions is stronger than that under stable and neutrally stratified conditions. Although their models have been verified with high accuracy and applied in many pieces of research, the derivation process of the elliptical wake model is still lacking. Furthermore, the analytical wake model is widely developed and adopted due to its simplicity, and thus, one of the most important things worth noting is to avoid complex and computationally expensive calculations to determine some empirical parameters like expansion rate before its application. However, this method has been widely employed in previous models.

The purpose of this paper is to develop an easy-to-use three-dimensional elliptical Gaussian shape wake model (3DEG model). The main contributions with respect to conventional models are as follow: (1) Multivariate Gaussian function with anisotropic standard deviations is adopted in derivation process instead of the standard Gaussian function with a uniform standard deviation, (2) the wind shear effect is combined with the proposed elliptical wake model to reflect the 3D effect, (3) the universal expression of wake expansion rate in each dimension is given. For clarity, a flowchart of the present research is demonstrated in Fig.1.

The paper is organized as follows. In section 2, the basic assumptions and derivation process are discussed in detail. The 3DEG wake model with uniform inflow (3DEG-U model) is developed first and then converted into a 3DEG wake model by considering the shear effect. Then, the expressions of wake expansion rate are proposed and validated. In section 3, the comparison and validation of the proposed 3DEG wake model are carried out using four series of experimental data. In section 4, key findings and conclusions of this study are summarized. The present model is capable of predicting the wake profiles of any given wind turbine. By considering the anisotropy of wake boundary in each dimension, this model can provide more reliable results when estimating the power generation of wind farms. Therefore, it can contribute to wind farm optimization and carbon neutrality.

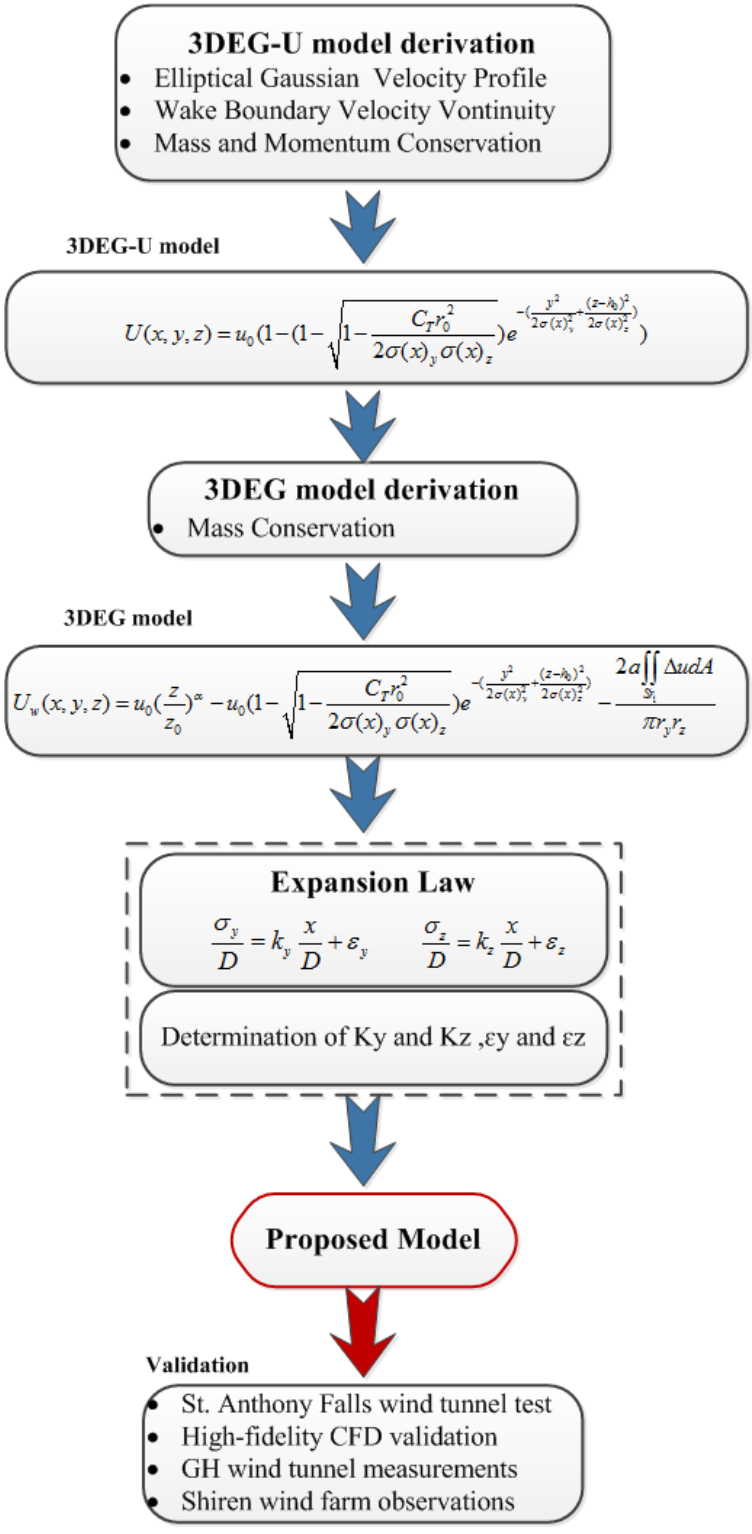

Fig.1 The work flowchart of this study.

2. Model derivation

To demonstrate the spatial location clearly, the 3D coordinate system is established first. As shown in Fig.2, the positive x-axis direction denotes the downstream direction. The Y-axis

refers to the radial direction in the horizontal level and is perpendicular to the inflow direction. The positive Z-axis direction is the vertical direction and perpendicular to the ground up. The coordinate origin is set at the bottom of the wind turbine tower, and thus, the coordinate point at the hub center is (0, 0, h_0).

The derivation process of the 3D elliptical Gaussian shape wake model is mainly divided into 3 steps. Firstly, the 3DEG wake model with uniform inflow assumption (3DEG-U model) will be developed based on the multivariate Gaussian function. The second step is to convert it into the 3DEG model by the means of replacing uniform inflow in the first step with a shear wind profile. Finally, the wake expansion rates in the horizontal and vertical directions are derived. To the best of our knowledge, it would be the first empirical expression of wake expansion rate in the vertical direction.

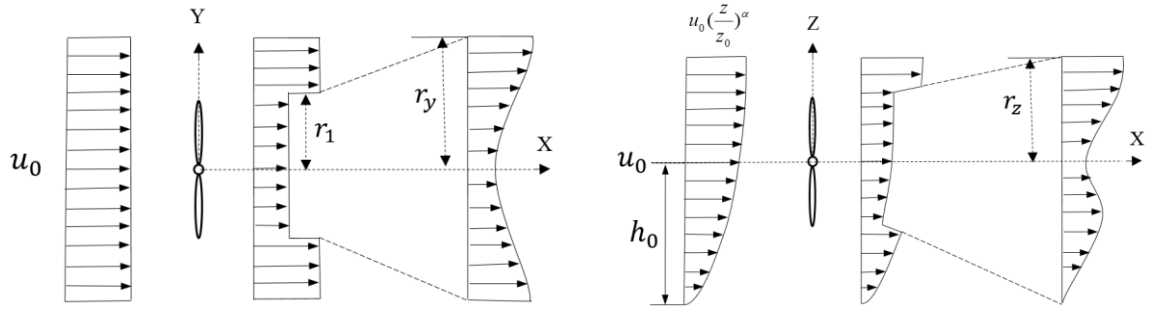

(a) Horizontal plane (b) Vertical plane

Fig.2 Schematic diagram of wake expansion in the vertical and horizontal direction.

2.1 Derivation process of 3DEG-U wake model

In order to develop a 3DEG wake mode, a 3DEG-U model needs to be derived first because the wind shear function $u_0(\frac{z}{z_0})^\alpha$ cannot be integrated into Eq. (5) [32]. Therefore, the shear inflow profile is replaced by the uniform inflow u_0 measured at the height of h_0. The wake velocity in the 3DEG-U model is defined as $U(x, y, z)$. To characterize the wake distribution, two basic assumptions are demonstrated below:

(1) The wake velocity downstream is Gaussian shape. Note that in order to establish a 3D elliptical wake model, an anisotropic 2D Gaussian probability density function should be employed in the YZ plane from the beginning to derive. The velocity distribution could be expressed as follow:

$$U(x,y,z)=u_0-\frac{A(x)}{2\pi\sigma(x)_y\sigma(x)_z}e^{-(\frac{y^2}{2\sigma(x)_y^2}+\frac{(z-h_0)^2}{2\sigma(x)_z^2})} \quad (1)$$

In Eq. (1), A is the unknown parameters that need to be determined. $\sigma(x)_y$ and $\sigma(x)_z$ are standard deviation in horizontal (Y) direction and vertical (Z) direction, respectively.

From the properties of Gaussian distribution, the good predictive ability of the wake model could be obtained by specifying a wake radius equal to 2.58σ in one-dimensional Gaussian distribution to represent a probability of 99% [20]. When 2D Gaussian distribution is employed, the confidence region actually changes from a line segment to an ellipse. In order to also represent the 99% probability in the area, each dimension needs to meet the probability of 99% square root. According to the standard density function curve of two-dimensional Gaussian distribution, 2.81 standard deviations ($2.81\ \sigma$) in each dimension away from the mean value satisfy this requirement. Consequently, the relation between standard deviations and wake boundary can be established:

$$r_y=2.81\sigma(x)_y \quad (2)$$

$$r_z=2.81\sigma(x)_z \quad (3)$$

(2) The wake flow follows the mass and momentum conservation law [32]. The same assumption was used in the BPA model [23] by neglecting pressure terms and viscous in the momentum equation.

$$\rho\int U(x,y,z)[u_h-U(x,y,z)]dA=T \quad (4)$$

where T is the thrust force and can be expressed as [33]:

$$T=\frac{1}{2}C_T\rho A_0{u_0}^2 \quad (5)$$

where C_T denotes the thrust force coefficient and A_0 is the swept area of the rotor.

The next step is to find A. By using the same method mentioned in Ref. [23], Eq.(1) and Eq.(5) are inserted into Eq.(4) to obtain an equation about parameter A and express as:

$$\frac{1}{4\pi\sigma(x)_y\sigma(x)_z}A^2-u_0A+\frac{1}{2}C_TA_0{u_0}^2=0 \quad (6)$$

By solving the equation above, two values of A can be obtained while only one is physically correct since it needs to fulfill a smaller velocity at a longer downstream distance. It could be expressed as:

$$A = 2\pi\sigma(x)_y \sigma(x)_z u_0 (1 - \sqrt{1 - \frac{C_T r_0^2}{2\sigma(x)_y \sigma(x)_z}}) \tag{7}$$

Combining Eq. (1) and Eq. (7), the elliptical Gaussian shape wake model with uniform inflow can be derived:

$$U(x,y,z) = u_0 (1 - (1 - \sqrt{1 - \frac{C_T r_0^2}{2\sigma(x)_y \sigma(x)_z}}) e^{-(\frac{y^2}{2\sigma(x)_y^2} + \frac{(z-h_0)^2}{2\sigma(x)_z^2})}) \tag{8}$$

2.2 Derivation process of 3DEG wake model

In the first step above, the inflow speed difference in the vertical direction is neglected. In the second step, the simplified 3DEG model is upgraded by considering the wind shear effect. The uniform inflow results in a Gaussian-shape wake speed distribution downstream, which is symmetrical. On the contrary to uniform inflow, the shear inflow is asymmetrical and surely results in asymmetrical wake speed distribution. Actually, its distribution is a combination of Gaussian shape and shear distribution. To derive the 3DEG wake model, the wind power law is applied to calculate the speed difference Δu (see Fig.3 (a)) between shear wind and uniform wind.

$$\Delta u = u_0 (\frac{z}{z_0})^{\alpha} - u_0 \tag{9}$$

The existing speed difference Δu in inflow wind results in a corresponding mass difference Δm (see Eq. (10)) in wake flow. The mass variation in vertical direction decomposes the originally axisymmetric wake distribution and it therefore needs to be taken into account to derive the 3DEG model. Note that in order to calculate the mass variation in a 3D model, the corresponding speed should be adopted to integrate the area. It should also be noted that $\Delta u(1-2a)$ refers to the far-wake speed corresponding to the area swept by the initial wake radius r_1, which is reasonable since only wake characteristics beyond near wake deserve attention in most cases.

$$\Delta m = \iint_{Sr_1} \Delta u(1-2a)dA + \iint_{S_{elliptical}-Sr_1} \Delta u dA \tag{10}$$

In which, $S_{elliptical}$ refers to the elliptical wake area at any downstream with a long radius r_y and a short one r_z. r_1 is initial wake radius and it can be expressed as [20]:

$$r_1 = r_0\sqrt{\frac{1-a}{1-2a}} \tag{11}$$

where r_0 denotes the wind turbine rotor radius. a denotes the axial induction factor, which can be calculated by the thrust coefficient C_T.

$$a = \frac{1-\sqrt{1-C_T}}{2} \tag{12}$$

To distinguish the 3DEG model from the 3DEG-U model ignoring the shear effect, the 3DEG model is designated as $U_w(x,y,z)$. By applying mass conservation law in the wake flow and substituting Eq.(10) into Eq. (13), as shown in Fig.3, the 3DEG wake model (see Eq. (14)) can be derived based on the 3DEG-U model developed in the first step.

$$\iint_{S_{elliptical}} U_w(x,y,z)dA = \iint_{S_{elliptical}} U(x,y,z)dA + \Delta m \tag{13}$$

$$U_w(x,y,z) = u_0\left(\frac{z}{z_0}\right)^{\alpha} - u_0\left(1-\sqrt{1-\frac{C_T r_0^2}{2\sigma(x)_y\sigma(x)_z}}\right)e^{-\left(\frac{y^2}{2\sigma(x)_y^2}+\frac{(z-h_0)^2}{2\sigma(x)_z^2}\right)} - \frac{2a\iint_{Sr_1}\Delta u dA}{\pi r_y r_z} \tag{14}$$

This wake model is closer to reality as it is truly dependent on z and y and considers the shear effect. To the best of our knowledge, it has not been adopted by any other analytical wake mode. Using the proposed 3DEG wake model, one can calculate the wake speed $U_w(x,y,z)$ at any downstream spatial position in a simple and fast manner.

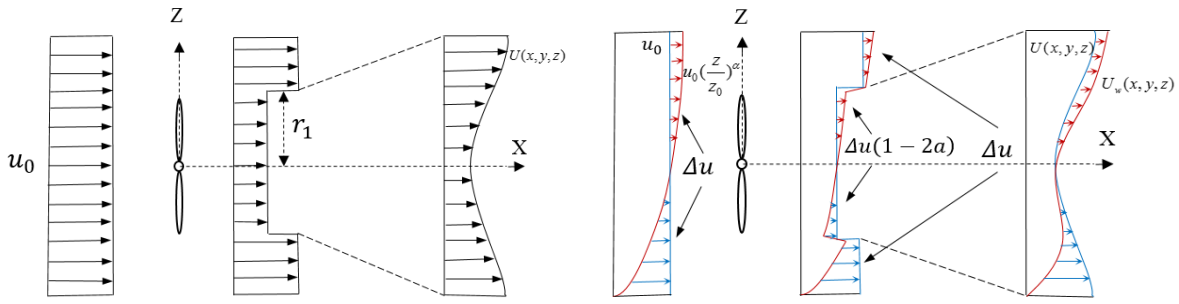

(a) 3DEG-U model (b)3DEG model compared with 3DEG-U model

Fig.3 Velocity distributions in the vertical direction of the 3DEG-U model and 3DEG model, respectively.

2.3 The determination of expansion rates

The anisotropy in the wake expansion rate in the vertical and horizontal directions has been verified by Xie [17] and Abkar and Porté-Agel [30]. The wake radius at the same downstream distance is larger in the horizontal direction than that in the vertical direction and the discrepancy increases with distance. Thus, the wake distribution in the YZ plane shows a more elliptical Gaussian shape than a circular one. This is mainly attributed to the fact that ambient turbulence in the horizontal direction is larger than it in the vertical direction, speeding up the mixing process of wake and free flow in the horizontal plane, and thus, boosting wake recovery. Consequently, two standard deviations are needed and their growth rates need to be determined.

It is worth noting that there are two kinds of wake expansion rates with different physical meanings. In the wake model of Jensen [12], Gao [31], Sun [26] and Ge [21], expansion rate k refers to the growth rate of physical wake boundary, while in the wake model of Bastankhah [23], Xie [17] and Ishihara [28], expansion rate k^* signifies the growth rate of standard deviation. In this paper, k_y and k_z are deployed with the same physical meaning of the expansion rate $k^*=\partial\sigma/\partial x$ and can be expressed as:

$$\frac{\sigma_y}{D}=k_y\frac{x}{D}+\varepsilon_y,\ \frac{\sigma_z}{D}=k_z\frac{x}{D}+\varepsilon_z \tag{15}$$

where D denotes the rotor diameter of wind turbine. ε_y and ε_z are equal to the value of $\frac{\sigma_y}{D}$ and $\frac{\sigma_z}{D}$ respectively as downstream distance approaches to zero.

According to the anisotropy of expansion rate validated by Xie [17] and Abkar and Porté-Agel [30], different k^* and ε in two directions need to be determined. However, a specific expression of k^* was not proposed, and then the authors got different specific values of k^* for different cases by fitting the LES results. This makes the above elliptical models alone insufficient to predict the wake distribution since a high computational-cost simulation must be carried out to determine the expansion rate in an analytical model known for its good

accuracy and efficiency. In this study, inspired by Ishihara [28], k_y and k_z, ε_y and ε_z are modeled as a function of C_T and I_0. It is worth noting that, as concluded in Ref. [30] as well as commented in the study, it would be better to consider turbulence intensity in all three directions. However, in practice, turbulence intensity in three directions is unavailable in most cases. Furthermore, the expression of expansion rate is essentially a semi-empirical formula, which has no physical meaning behind the empirical relation, so it cannot reflect the relationship between the three turbulence intensities. Therefore, only the ambient streamwise turbulence intensity at hub height is employed in this model for its universality. In order to obtain constants in these parameters, LES cases from Ref. [17] and [30] are adopted. In which, C_T ranges from 0.375 to 0.8 and I_0 ranges from 0.05 to 0.11. Finally, the empirical expression of k_y and k_z, ε_y and ε_z are proposed by data fitting with all R-squares above 0.9 and presented in Eq. (16) and (17).

$$k_Y = 0.065 C_T^{\,0.2566} I_0^{\,0.2808},\ k_Z = 0.0866 C_T^{\,0.4279} I_0^{\,0.4707} \tag{16}$$

$$\varepsilon_Y = 0.2406 C_T^{0.1147} I_0^{0.0124},\ \varepsilon_Z = 0.2788 C_T^{0.0295} I_0^{0.032} \tag{17}$$

So far, the 3DEG wake model is completely developed and the equations are highly simple with a little requirement of computing resources. Based only on the inflow conditions and turbine parameters, the 3DEG model is able to calculate the three-dimensional velocity profile in the wake $U_w(x, y, z)$ for any given wind turbine within a few seconds.

3. Model validation

The proposed 3DEG wake model is validated through four cases including measured data from two wind tunnels, one field experiment and one LES results from the literature. For comparison, additional four typical wake models are selected, including one-dimensional Jensen model[34], two-dimensional Gaussian-shape wake model from Ge [21] (2DGe model hereafter), three-dimensional Gaussian-shape wake model from Sun [26] (3DSun model hereafter) and BPA model [23]. The characteristics and expressions of these four models as well as the 3DEG model are listed in table 1. In which, k_{Jensen} in 1D Jensen model is the wake expansion rate, which is recommended to be 0.075 [35] for the onshore turbine and 0.04 [36] for the offshore wind turbine. For the 2DGe model, J=1 and k=0.075 are adopted according to Ref. [21]. C in 3DSun model and wake expansion rate $k^*=\partial\sigma/\partial x$ in BPA model need to be adjusted for different wind turbine wake cases.

It should be highlighted that since 1D Jensen model and 2DGe model can only deal with uniform inflow, these two models are specifically employed in horizontal wake profiles comparison. While 3D models are able to reflect the wake distribution in vertical direction with sheared inflow conditions, consequently, 3DSun model and BPA model are qualified to make the comparison with the 3DEG model.

Table 1 Summary of typical wake models

Wake model	Characteristic	Expression
Jensen model[34]	1D; top-hat shape	$u_{Jensen} = u_0[1-2a/(1+k_{Jensen}x/r_0)^2]$
2DGe model[21]	2D; Gaussian shape	$\frac{\Delta U(x,r)}{U_\infty} = \left(1-\sqrt{1-\frac{2J^2C_T}{\left(k\frac{x}{r_0}+1\right)^2}}\right)\exp\left(\frac{2J^2}{\left(k\frac{x}{r_0}+1\right)^2}\left(\frac{r}{r_0}\right)^2\right)$
3DSun model[26]	3D; Gaussian shape	$U(x,y,z) = A(x)\left(\frac{1}{2\pi\sigma(x)^2}e^{-\frac{y^2+(z-h_0)^2}{\sigma(x)^2}}\right)+B(x)+U_0(z)$ $\begin{cases} A(x) = \frac{Q(x)-\int_{h_0-r_w(x)}^{h_0+r_w(x)} 2\sqrt{r_w(x)^2-(z-h_0)^2}U_0(z)dz}{\left(1-e^{-\frac{C^2}{2}}-\frac{C^2}{2}e^{-\frac{C^2}{2}}\right)} \\ B(x) = -\frac{A(x)C^2}{2\pi r_w(x)^2}e^{-\frac{C^2}{2}} \end{cases}$
3D BPA model[23]	3D; Gaussian shape	$\frac{\Delta U(x,r)}{U_\infty} = \left(1-\sqrt{1-\frac{C_T}{8(\sigma/D)^2}}\right)\exp\left(-\frac{1}{2(\sigma/D)^2}\left\{\left(\frac{z-z_h}{D}\right)^2+\left(\frac{y}{D}\right)^2\right\}\right)$ $\sigma/D = k^*x/D+\varepsilon$
3DEG model	3D; elliptical Gaussian shape;	$U(x,y,z) = u_0(\frac{z}{z_0})^\alpha - u_0(1-\sqrt{1-\frac{C_T r_0^2}{2\sigma(x)_y\sigma(x)_z}})e^{-(\frac{y^2}{2\sigma(x)_y^2}+\frac{(z-h_0)^2}{2\sigma(x)_z^2})} - \frac{2a\iint_{S_1}\Delta u dA}{\pi r_y r_z}$ $\sigma_y/D = k_y x/D+\varepsilon_y,\ \sigma_z/D = k_z x/D+\varepsilon_z$

3.1 Validation by the wind tunnel tests from St. Anthony Falls Laboratory

Firstly, the vertical and horizontal profiles of velocity in the wake are validated by the measured data in the St. Anthony Falls wind tunnel test [9]. The test was conducted under neutrally-stratified boundary layer condition in a wind tunnel with a main test section fetch of 16m. A high-resolution hot wire anemometry was used to collect velocity data in wake flow.

The miniature wind turbine in this test consisted of a three-blade GWS/EP-60X3 rotor attached to a small DC generator. The radius of the rotor blade is 0.075 m and the hub height of the wind turbine is 0.125 m. As for the inflow condition, the inflow velocity was characterized by turbulence intensity of 7 %, velocity at the hub height of 2.2 m/s, and wind speed power law exponent of 0.146.

Fig. 4 shows the comparison of the vertical profile of velocity in wake with measured data [9], CFD results [9], and the wake models mentioned in Table 1 at four downstream locations. The wind turbine is located at x=0 and the tower bottom is the origin of the coordinate. Fig. 4(a) is at the x=5D (D refers to the diameter of the tested wind turbine) downstream distance; (b) is at the x=7D downstream distance; (c) is at the x=10D downstream distance and (d) is at the x=14D downstream distance. The vertical axis refers to the dimensionless ratio of z distance and rotor diameter D and the horizontal axis represents the wind velocity in the wake.

As illustrated below, the proposed 3DEG model is able to predict the vertical wake profile well in all downstream locations. The maximal wake deficit appears at the centerline and recovers as it leaves the center area due to its mixing with the higher velocity free stream. Note that it seems that the minimum wake velocity near the hub appears slightly below the hub height instead of the exact hub height, especially in Fig .4(a) and (b), but the maximal wake deficit does appear at hub height after verification by the authors. This phenomenon is related to the fact that the vertical distribution of wake is the effect produced by the combination of Gaussian distribution and wind shear profile. On the other hand, the other two models both adopt the standard Gaussian assumption to describe the wake distribution. Among them, the 3DSun model initially overestimates the maximal wake deficit at 5D but fits the wake profile at 7D very well and then slightly underestimates the wake deficit around hub center at farther downstream distances. It seems that the 3DSun model has a faster growth rate than measured data in this case. For BPA model, the prediction results marginally overestimate the experimental value while having a larger gap around the hub and bottom height. The disparity around the wake center decreases with the increase of downstream distance and becomes negligible after 10D. Therefore, the overall performance of BPA model is favorable as well. The only problem is that the wake expansion rate in BPA model $k^{*}=\partial\sigma/\partial x$ must be determined by CFD and the computational cost of which could be quite high.

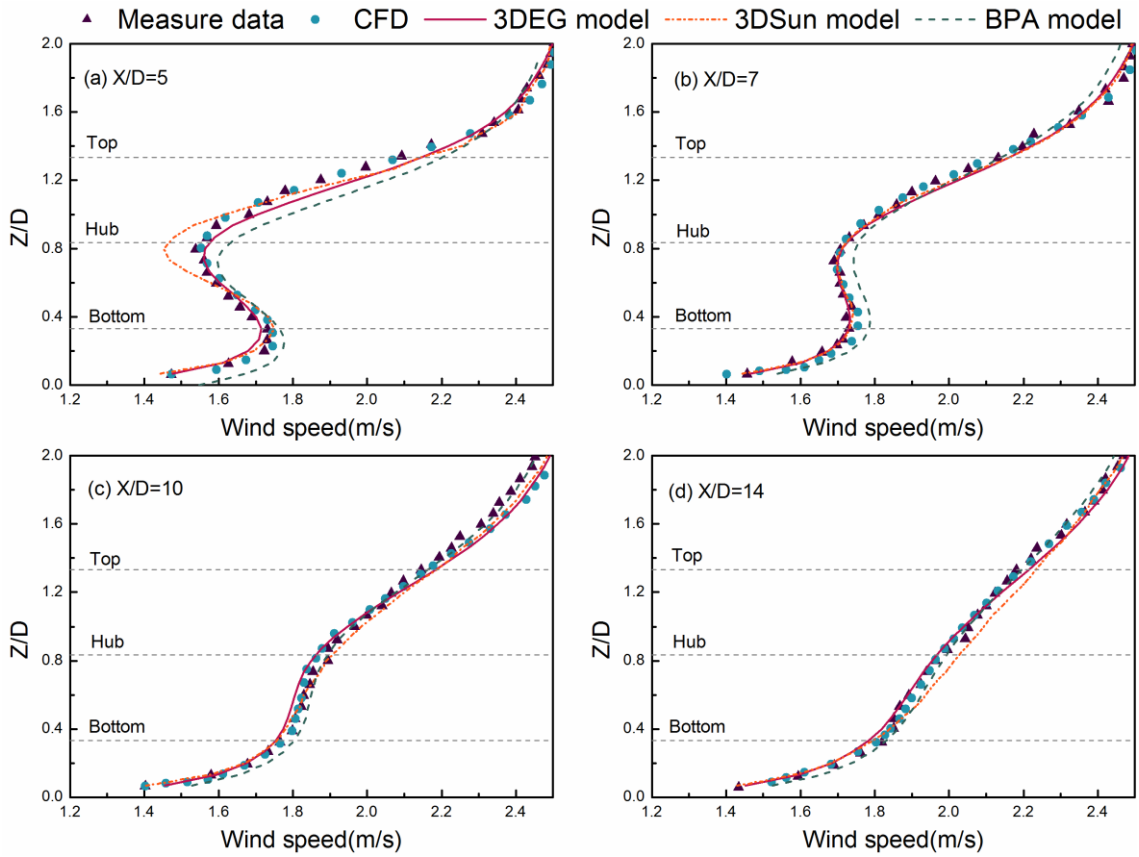

Fig.4 Comparison of vertical profiles of wake velocity between the measured data and the predicted results of different wake at four downstream locations.

To quantify the prediction ability of the proposed 3DEG wake model, the relative error δ is introduced in this study:

$$\delta_i = \frac{U(x,y,z)_i - U_{\exp i}}{U_{\exp i}} \times 100\% \tag{19}$$

$$\delta = \sqrt{\frac{1}{n}\left(\sum_{i=1}^{n} \delta_i^2\right)} \tag{20}$$

where δ_i refers to the relative error of the i_{th} measured data at each downstream distance in the wake; $U(x,y,z)_i$ and $U_{\exp i}$ represent the corresponding wake velocities calculated by the 3DEG model and measured by wind tunnel test, respectively.

In general, the relative error in Table 2 demonstrates that the present model achieves a high level of accuracy. Relative errors at all downstream locations are within 2.5%. Among them, the biggest error 2.35% appears at 5D while the smallest error 1.05% appears at 14D where wake distribution gradually recovers to the inflow wind profile. The relative errors of

3DSun model and BPA model are also comparatively small. Although a certain degree of inaccuracy at the hub height appears at 5D and therefore owning the largest error compared with downstream locations, the overall error is acceptable.

The specific relative error at each measured spatial position is also analyzed. As illustrated in Fig. 5, the prediction is reasonably good for each height at different downstream. In particular, the present model runs quite well and stably around the hub height with errors within -2% ~ 3% in all four distances, which is of great importance because it means the accuracy of forecasting the maximal wake deficit. In the area above the hub height, relative errors at all locations experience the trend of up and down. Among them, errors at 5D have the largest fluctuation featured with two errors beyond 5%, however, most spatial positions have errors within ±5%. Besides, most errors around the tip height are positive, which indicates that the 3DEG wake model tends to predict the wake velocity greater than the reality around this part.

Table 2 Relative errors of the compared models in different downstream distance

Downstream distance	5D	7D	10D	14D
3DEG relative error	2.35%	1.44%	1.70%	1.05%
3DSun relative error	3.11%	1.04%	1.27%	1.72%
BPA relative error	2.96%	2.63%	2.27%	1.75%

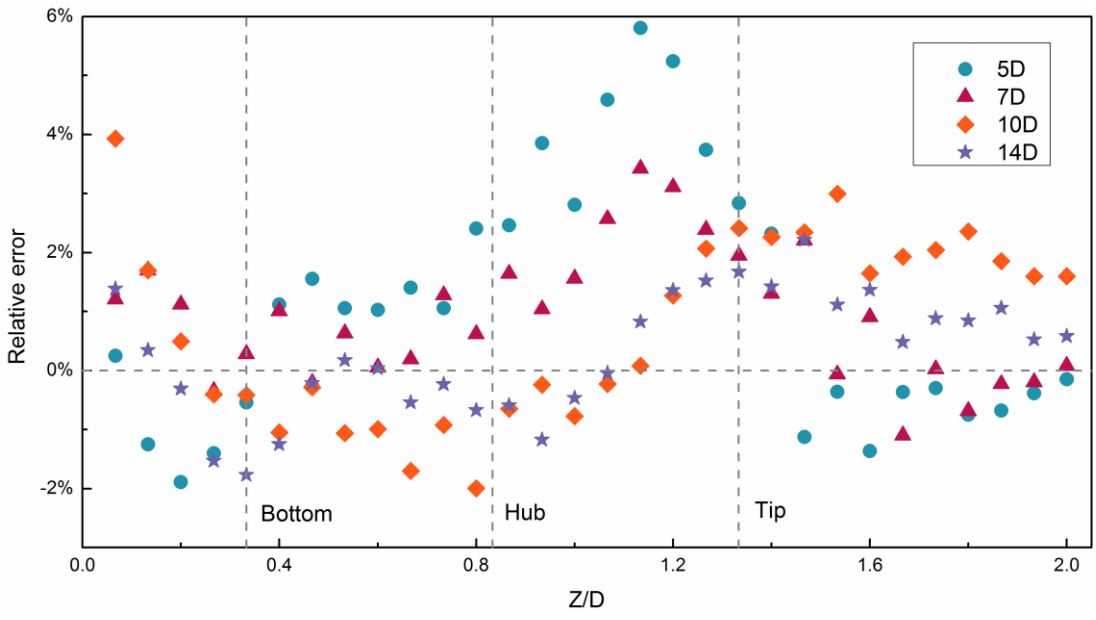

Fig.5 Relative errors in vertical profiles of the 3DEG model compared with St. Anthony Falls wind tunnel test.

For the completeness of validation, contour lines of wake velocity in YZ plane at downwind location x/D=5 are compared and shown in Fig. 6, of which (a) is measured data also from Ref. [9], (b) is calculated by the proposed 3DEG model at the same position. By contrast, the contour lines predicted by the 3DEG model agree well with measured data. In particular, the present model can apparently predict wake magnitude well in horizontal direction. Please note that the center of the contour lines of experimental data is exactly not on the Y/D=0 line but about 1D to the left. There is only a slight underestimation near the bottom height in horizontal level centralized within ±0.3D, which is consistent with the results shown in Fig. 4(a). It is of interest that, due to taking into account the wind shear effect, the wake contour lines in Fig.6 (a) and (b) show non-axisymmetrical concerning horizontal plane with the center lower than the rotor center, which is different compared with uniform inflow. By contrast, the proposed 3DEG wake model is capable of accurately predicting both the vertical and horizontal wake profiles compared against the wind tunnel experimental data of a miniature wind turbine.

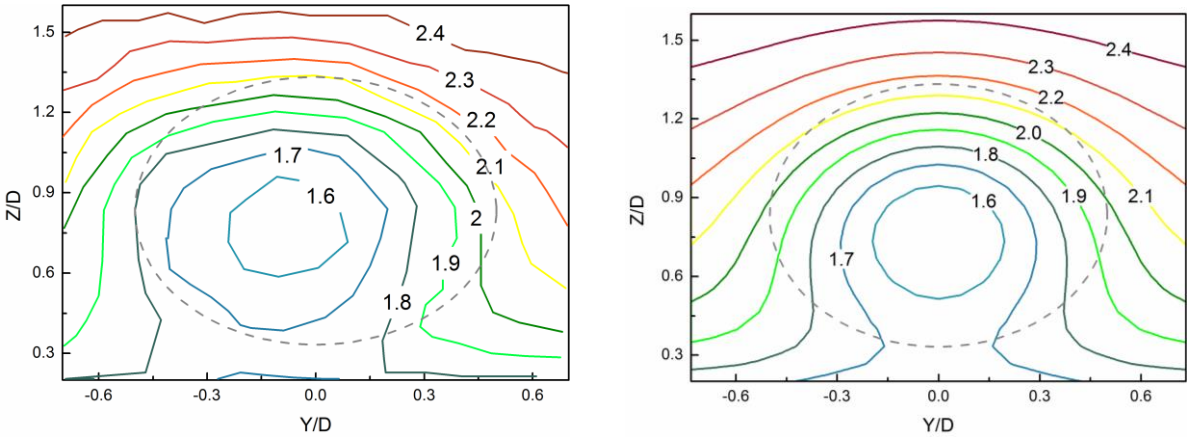

(a) Measured data in wind tunnel (b) prediction from 3DEG model

Fig.6 Wake velocity in YZ plane at downstream location x/D=5 (dash line is the rotor swept area)

3.2 Validation by the data from LES results of a Vestas V80−2MW wind turbine

Abkar and Porté-Agel [30] conducted a series of high-fidelity simulations with LES to investigate the impact of atmospheric stability on wind turbine wakes. The results under neutrally stratified atmospheric boundary layer are deployed here for comparison. The

incoming flow speed at hub height is 8m/s with a power law exponent of 0.173. The ambient turbulence intensity almost linearly decreases with the increase of height. However, as mentioned in *2.3 The determination of expansion rates*, for its universality, only the streamwise turbulence intensity at hub height with a value of 11% is used to represent the ambient turbulence. The modeling object is a widely reported Vestas V80-2MW wind turbine [23,37], of which the rotor diameter is 80m and the height hub is 70m. The thrust coefficient corresponding to the test wind speed is 0.8.

In Fig. 7, the vertical profile of wake at various downwind locations predicted by the proposed 3DEG model is verified with LES data [30] and other comparable models. From these it can be seen that the present model is able to predict the wake distribution with favorable accuracy at all downstream locations. Note that almost at all downstream locations, the 3DEG model slightly overestimates the wake velocity around the top height and underestimates it below the bottom height. One possible explanation is that the streamwise turbulence intensity at hub height is adopted instead of the whole intensity profile used in LES calculation [30]. As mentioned above, the turbulence intensity decreases along with the increase of height. In fact, a lower value of turbulence intensity above hub height results in a slower process of wake recovery, whereas an underestimation below the hub height is caused by a greater turbulence intensity than used. However, as the downstream distance increases, so does the accuracy with which the proposed model forecasts the velocity deficit. Combined with the prediction of the 5D vertical wake distribution in the first case, it can be reasonably inferred that the wake distribution with a downstream distance of more than 4D can achieve a good consistency. In the 3DSun model, C=2.83 is adopted. Like the 3DEG model, at 4D, this model also overestimates the wake velocity above the hub height and underestimates it around the bottom height, but with a larger gap. As the distance increases, the 3DSun model shows an apparent underestimation of wake distribution, especially between the top and bottom. Even after 16D, the prediction results of other models are almost the same as the LES value, while the 3DSun model still has noticeable disparity. For BPA model, obvious underestimation appears around the wake center at 4D, which may be related to limitations of the standard Gaussian assumption. In Ref. [30], the authors employed the two-dimensional elliptical Gaussian to take into account the different horizontal and vertical wake expansion rates. In the meantime, the wake expansion rate for standard Gaussian function was also calculated in Ref. [30] and adopted in this paper for comparison. It can be concluded that the

difference between using these two assumptions is initially large and then becomes smaller as downstream distance increases, which is consistent with Ref. [30].

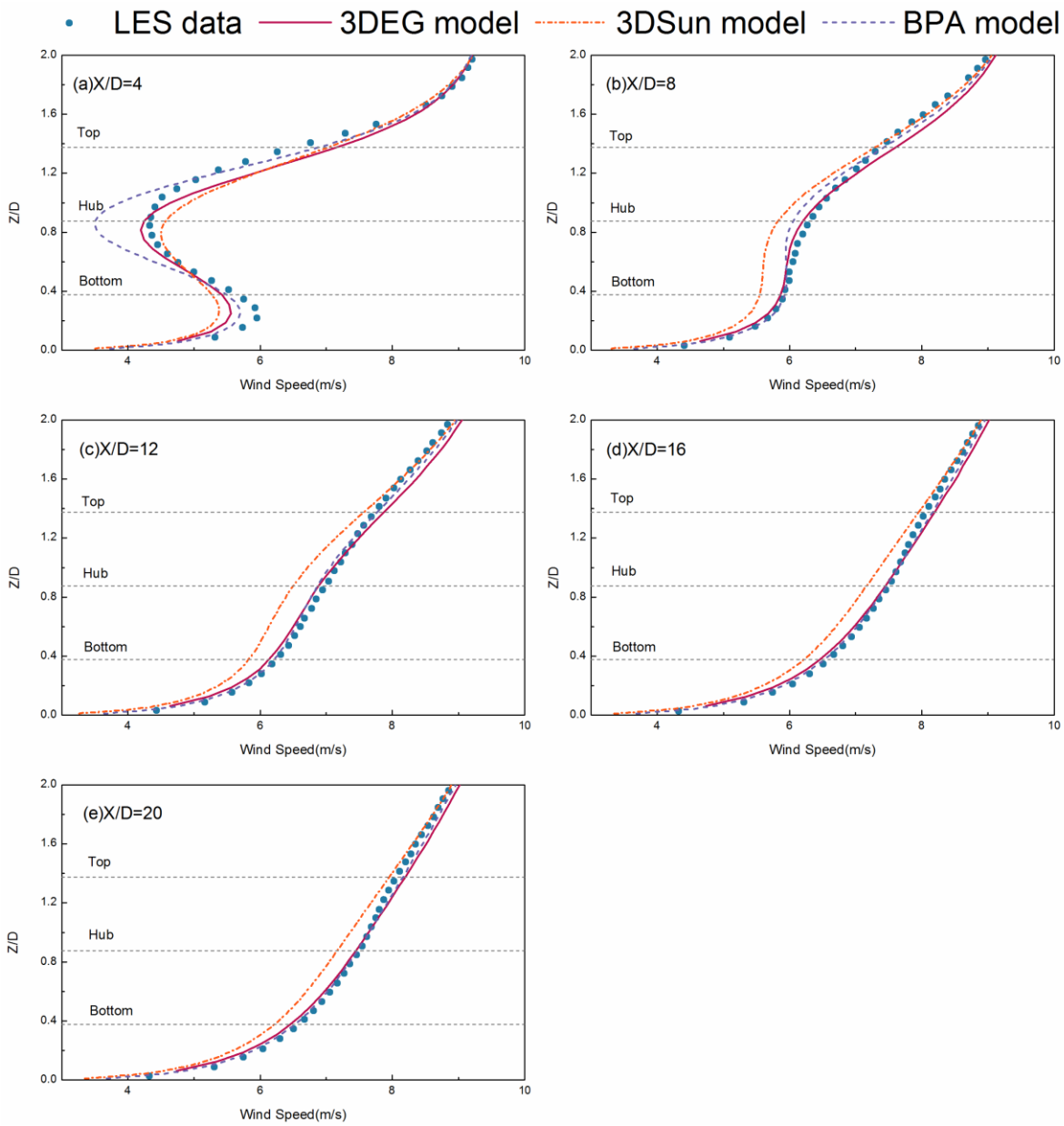

Fig.7 Comparison of vertical profiles of wake velocity between the LES data and the predicted results of different wake at five downstream locations

Relative error at each location is calculated by Eq. (19) and (20) and displayed in Table 3. For the 3DEG model, the biggest error 5.72% appears at 4D and all farther downstream locations have relatively small errors with a range from 1.98% to 2.29%, which further verify the idea that the proposed model is capable of predicting the wake distribution of all downstream distances beyond near wake. It is worth mentioning that the relative errors of 3DSun model increase at first and then drop down from 4D to 20D, which is different from

the common situation that happened in the 3DEG model and BPA model. While the relative errors of BPA model are fairly small from 8D to farther distances, an error of 8.09% at 4D verifies the necessity of employing an elliptical Gaussian assumption in wake model like the proposed model.

The specific relative errors of the comparison results are also analyzed. The overall prediction is accurate and the errors are within an acceptable range. Fig. 8 shows that relative errors at almost all downwind locations experience a trend from negative to positive, which means that as the height increases, the model is likely to underestimate first and then overestimate. The reason may be that a constant turbulence intensity at hub height is employed to represent the ambient turbulence that actually decreases as the height increases, which means the variation of turbulence intensity in the vertical direction is ignored. Relative errors at 4D appear a large fluctuation above the hub height. Note that although the prediction of the 3DEG model at 4D shows some kind of inaccuracy, it can still play a good role in the prediction of the maximum wake deficit. Except for 4D, relative errors at almost all other farther distances are within ±5%, which enables the proposed model quite appealing.

Table 3 Relative error of the compared models in different downstream distances.

Downstream distance	4D	8D	12D	16D	20D
3DEG relative error	5.72%	2.12%	2.10%	1.98%	2.29%
3DSun relative error	5.89%	6.13%	6.01%	5.16%	4.89%
BPA relative error	8.09%	2.08%	1.27%	0.97%	1.35%

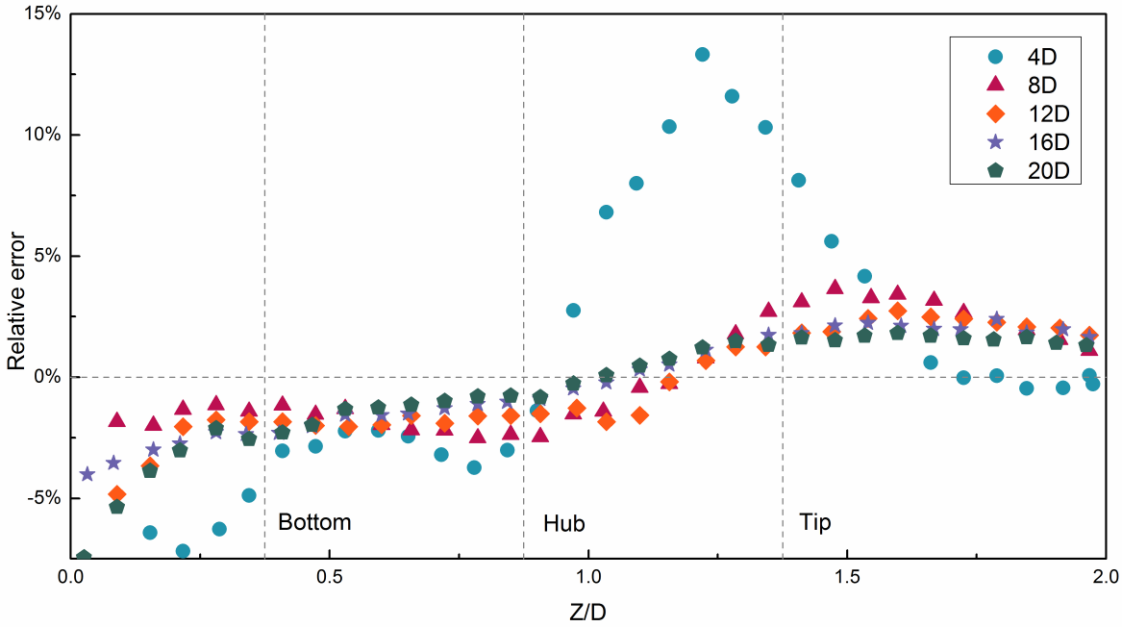

Fig.8 Relative errors in vertical profiles of the 3DEG model compared with LES results.

Fig. 9 shows the horizontal wake distributions at the same locations as the vertical profiles presented in Fig. 7. The Y-axis represents the wake velocity normalized by incoming flow at hub height and the X-axis is the normalized downstream distance. At X/D=4 downwind location, the present model is able to accurately predict the wake velocity around the hub and wake boundary while mildly overestimates it from ±0.2D to ±0.7D. As a simple analytical wake model, the 3DEG model lacks a clear description of the turbulence development mechanism, which may be the cause of the above problems. However, through the overall analysis of the velocity profiles of all downwind locations, it seems that this overestimation only happens in the relatively close downstream distance, which is out of concern in most cases. As demonstrated in farther downstream locations, the present model predicts the wake velocity with a favorable agreement in lateral areas. On the other hand, the 2DGe model apparently underestimates the wake distribution, especially around the wake center, although the discrepancy decreases as the downstream distance increases. The improvement of underestimation can also be noticed in the horizontal direction, from the center to sides, the disparity compared with LES results is continuously reduced. When approaching the wake boundary, the error is almost zero, which verifies that the “two sigma assumption” in 2DGe model [21] is reasonable.

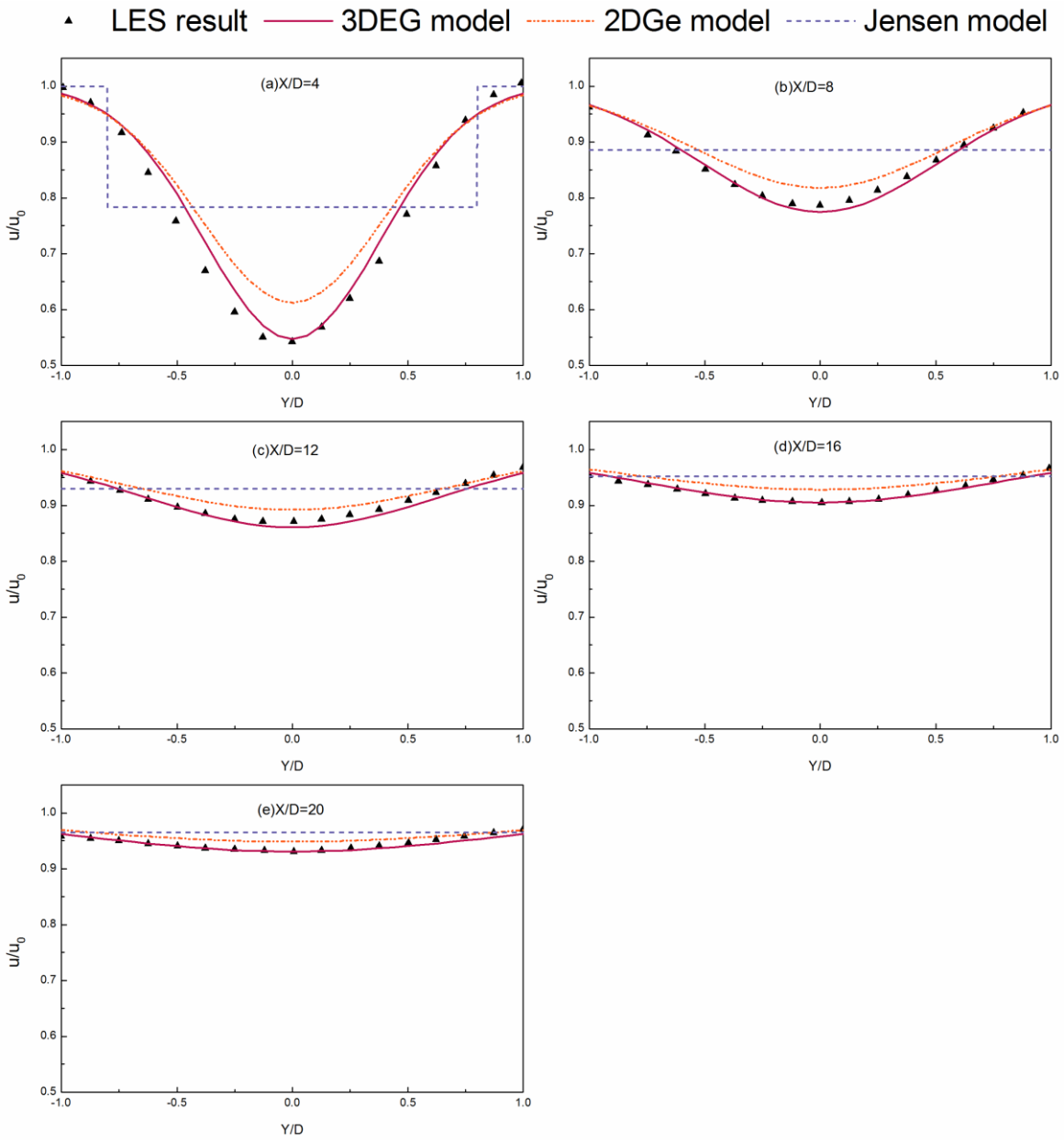

Fig.9 Comparison of horizontal normalized velocity in the wake between the LES data and the predicted results of different wake at five downstream locations.

Table 4 shows the relative error of the models for comparison in horizontal plane at five downstream distances. Like the same trend that appears in the vertical plane in Table 3, the relative error of 3DEG model drops dramatically as the downstream distance increases. The highest error is at 5D with a value of 3.77%, which is favorable. Compared with Table 3, results predicted by 3DEG model in horizontal direction have smaller relative errors at all downstream locations, which means the model predicts horizontal wake profiles more accurately. The relative error of 2DGe model is more than twice as large at 4D compared with the 3DEG model though it has acceptable results in the far wake region. The relative error of

Jensen model exceeds 20% at 4D and even reaches 7.6% at 8D, which proves that the top-hat assumption is far from reality and not eligible to describe wake distribution.

Spatial points calculated by 3DEG model are compared according to the LES calculation. Error analysis of the comparison results is visualized in Fig. 10. The largest error approaches to 8% in the 4D downstream distance and there are only another two errors that go beyond 5%. The relative errors at 4D experience a fluctuation on each side of the centerline, which implies that the present model is likely to predict the wake velocity larger than the reality at a relatively short downstream distance. All relative errors at other longer distances are quite small with a range from -3% to 2%. Therefore, the proposed 3DEG model is excellent at capturing the three-dimensional characteristics of the wake for a utility-scale wind turbine.

Table 4 Relative error of the compared models in different downstream distances.

Downstream distance	4D	8D	12D	16D	20D
3DEG relative error	3.77%	1.32%	1.00%	0.43%	0.48%
2DGe relative error	8.49%	2.73%	1.68%	1.81%	1.28%
Jensen relative error	21.86%	7.60%	4.14%	3.32%	2.40%

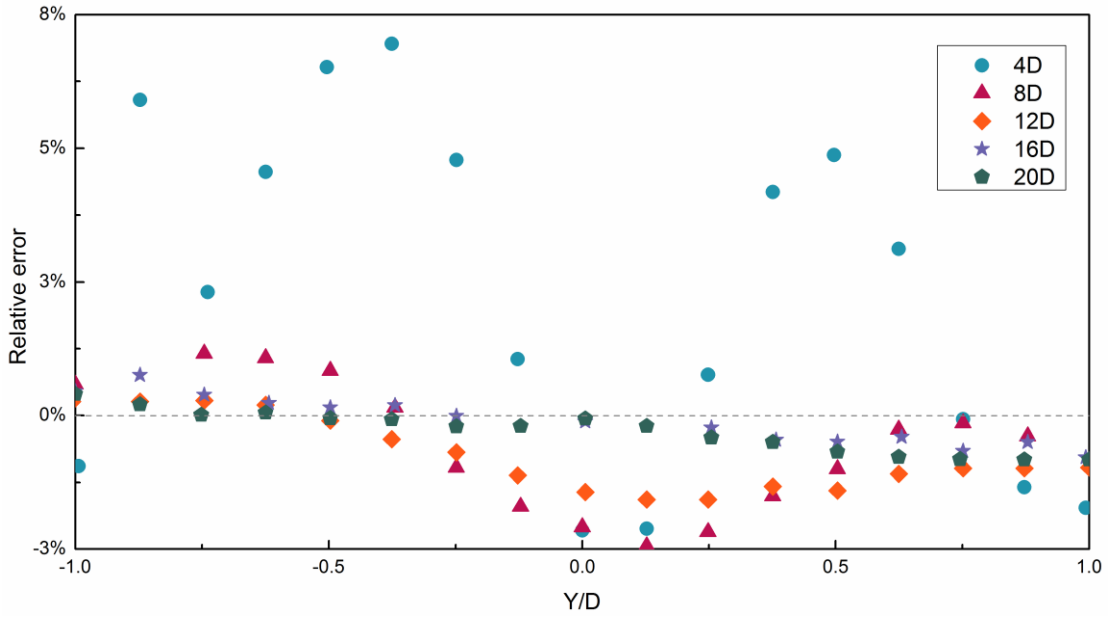

Fig.10 Relative errors in horizontal profiles of the 3DEG model compared with the LES results.

3.3 Validation by the measurements from GH wind tunnel experiment

A series of wind tunnel tests were carried out in an atmospheric boundary layer wind tunnel at the Marchwood Engineering Laboratories (MEL) by Garrad Hassan [38]. To model a flat terrain, the artificial surface roughness in the wind tunnel was set to be uniform with a roughness length of 0.075m. As for the target turbine, a 1/160 scaled horizontal wind turbine with realistic performance properties was tested. The rotor diameter of the full-scale wind turbine is 43.2m and the hub height is 50 m. The experiments were carried out with different tip speed ratios (TSR) for different planes, namely horizontal plane, centerline and vertical plane, respectively. In view of this situation, combined with the availability of experimental data, only horizontal measurements are used to verify the wake model. For the validation of horizontal plane, the test was performed under the hub-height inflow speed u_0=5.3m/s and TSR=2.9, with the corresponding thrust coefficient of 0.62.

Calculation of the velocity in the horizontal plane at various downstream distances from the proposed 3DEG model and other analytical models is compared with the measured data in Fig. 11. From these it can be noticed that the proposed wake model is able to reasonably predict the wake velocity in horizontal plane at the given hub height. At the 5D downstream distance, the velocity prediction is slightly lower around the centerline than measured data at the Y/D ration range of -0.25~0.25. At 7.5D and 10D, the model predicts lower values of wake velocity around the hub center as well, and greater values of wake velocity around the right side of the wake boundary at 7.5D. On the other hand, the 2DGe model and Jensen model can both predict the wake boundary at three locations with an acceptable agreement. However, the 2DGe model substantially underestimates the wake velocity though the gap is reduced as the downstream distance increases. As for the Jensen model, due to the top-hat assumption applied in this model, an obvious overestimation of the wake velocity near the edge of the wake as well as an underestimation of the velocity near the hub center are observed.

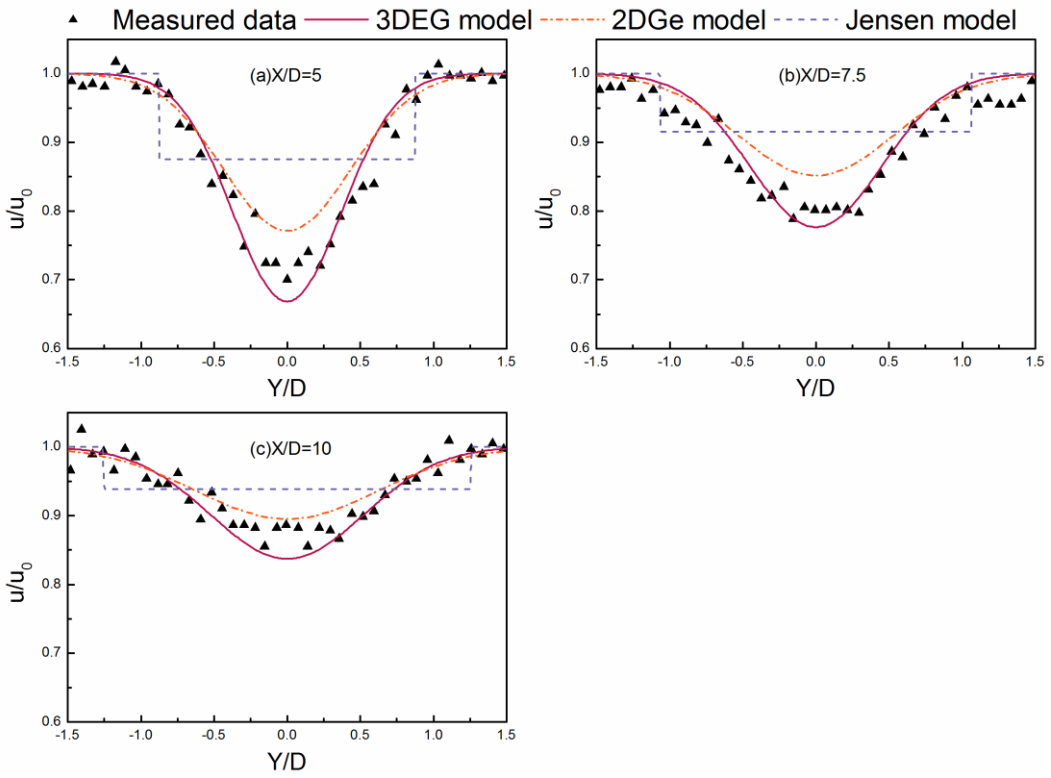

Fig.11 Comparison of horizontal normalized velocity in the wake between the measured data and the predicted results of different wake at three downstream locations.

The relative errors of the horizontal wake profiles predicted by several wake models are calculated and shown in Table 5. The accuracy of the forecast is favorable on the whole with the maximum error only reaching 2.96%. As the downstream distance increases, the relative error reduces and the 10D therefore has the smallest error with a value of 2.11%. Generally, the 3DEG wake model is more accurate at a far downstream distance. While the relative errors of 2DGe model are all within 5% and gradually decrease downstream, which seems to be acceptable in this case as well. Compared with other cases discussed in this paper, the relatively low discrepancy in terms of horizontal wake profiles may indicate that the 2DGe model is able to predict the wake of a miniature WT well but fails to calculate the velocity distribution after a real-scale WT. For the Jensen model, it is still cannot meet the accuracy requirements in the 7.5D range. Considering the distance between two WTs is typically around this range, the Jensen model can only provide rough predictions. By contrast, the accuracy and universality of the proposed 3DEG wake model are both validated.

Fig. 12 shows the relative errors at each specific location where measured data was collected. Only two errors exceed ±6% and both of them belong to the 5D downstream distance. Big errors at 5D are mostly centralized within the ±0.25D area, which implies that

the 3DEG model at 5D seems to overestimate the maximal wake deficit. The figure also illustrates that the present model predicts a lower value of wake velocity around the hub center at another two downstream locations. By observing the curves of measured data in Fig. 11(b) and (c), it can be found that the measurements around the hub center are significantly greater than the values on the adjacent sides at 7.5D and 10D. Note that theoretically, the largest wake deficit would exist at the hub center, namely, the wake velocity at the hub center should be lower than that of the adjacent sides and gradually recover in a Gaussian shape. A similar situation happens near the right wake boundary at 7.5D, where a sudden overestimation is found because the experimental data suddenly drops abnormally. The above analysis implies that some unstable errors may appear in the experiment process, and therefore, also make contributions to the inaccuracy.

Table 5 Relative error of the compared models in different downstream distances.

Downstream distance	5D	7.5D	10D
3DEG relative error	2.96%	2.67%	2.11%
2DGe relative error	4.61%	4.56%	2.30%
Jensen relative error	10.09%	7.62%	4.65%

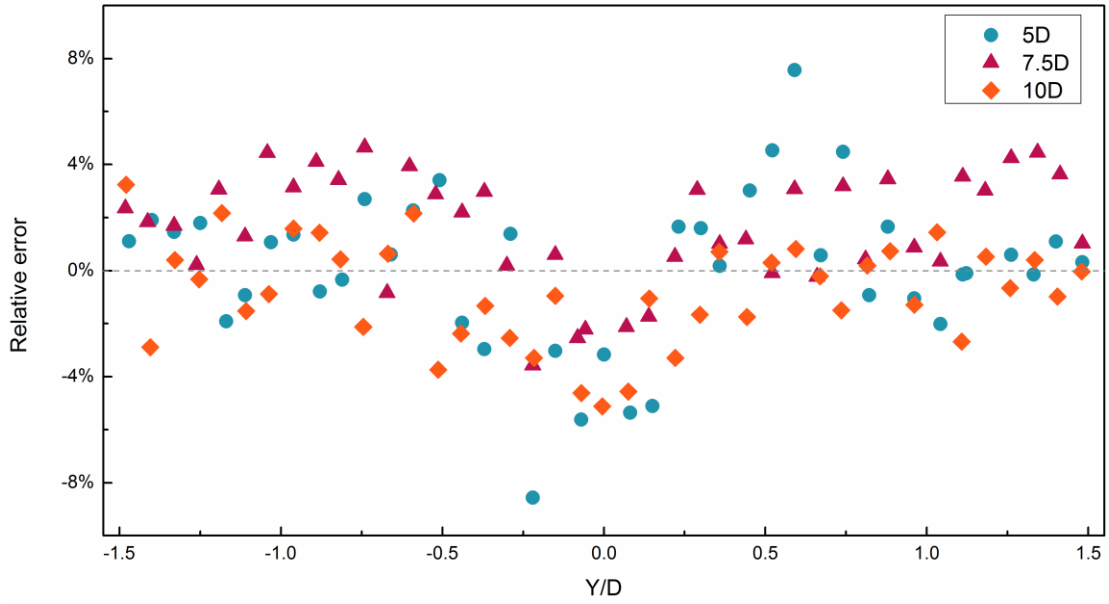

Fig.12 Relative errors in horizontal profiles of the 3DEG model compared with the GH wind tunnel test.

3.4 Validation by the field measurements from Shiren Wind Farm

Shiren Wind Farm, owned by Longyuan Power Group, is an onshore wind farm located in Zhangjiakou city, north of Hebei Province, China, with a total capacity of 75 MW. The plant consists of 50 WTs with a rated power of 1.5 MW, of which 33 WTs are AW77-1500 type manufactured by ACCIONA and 17 WTs are UP77-1500 type manufactured by United Power. The field measurements performed by our research group using LiDARs from December 2018 to June 2019 [31] are employed for this horizontal wake profile validation. Based on the main wind direction of northwest, a UP77-1500 wind turbine A10-2 with 77m rotor diameter and 65m hub height located at the north edge of the wind farm was selected as the target turbine (see Fig. 13), and there is no interference from other wind turbines downstream of 2000m (about 26D).

WindMast WP350 (WP350) and Wind3D 6000 (W3D6000) are two ground-based LiDARs deployed in this measurement to scan the incoming wind profile and wake velocity profile, respectively. The WP350 was located at 160m (approximately 2D) away from A10-2 in the northwest direction and the W3D6000 was placed at 1275m (approximately 16.5D) away from WT A10-2 in the southeast direction (see Fig. 13). The data measured from WP350 shows that the inflow speed at hub height is 9.35m/s with an average ambient turbulence intensity of 11%. By checking the thrust coefficient curve of WT A10-2[31], the thrust coefficient is 0.7 with respect to this inflow speed.

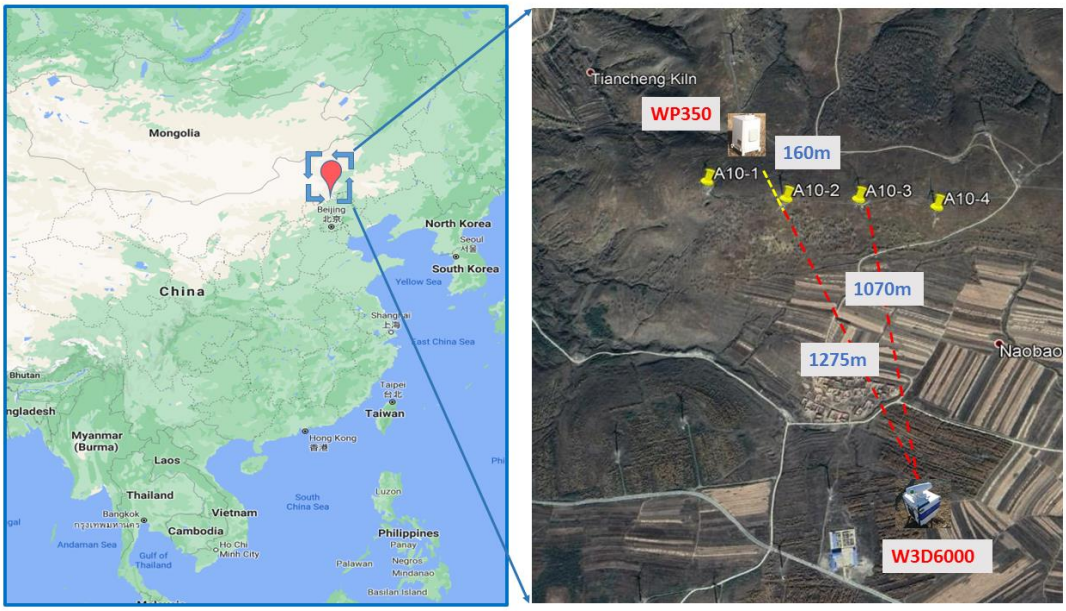

Fig. 13 Layout of the tested wind turbines in this validation measurement [31].

Fig. 14 shows the variation of normalized wake velocity in the horizontal direction at hub height, as a function of normalized lateral distance for the experimental data and proposed 3DEG wake model. The predictions obtained from the present model agree well with the measurements overall. At x=3D, the wake deficit around the wake center shows an overestimation, which is related to the fact that the mass conservation used in *2.2 Derivation process of 3DEG wake model* is based on the far-wake region assumption. The velocity in the near wake is actually greater than U(1-2a) and therefore 3DEG model predicts a lower value of velocity than measurement at 3D. As displayed in Fig. 14 (b)-(d), at any farther downstream locations, the present model is able to predict the maximal velocity deficit reasonably well and the wake profile in the far wake region. At 6D and 8D downstream distance, it is noticeable that although the predicted results fit experimental data pretty well at the hub center and the right side near the hub center, both sides show apparent disparity. Such disparity increases when approaching the wake boundary, which is more obvious in the farther downstream distance. This can be explained as the interference of the wake boundary between neighboring wind turbines. As illustrated in Fig. 14(c) and (d), since 6D, the wake radius expands and starts to interfere with each other from the wake boundary to the inside area, which results in an underestimation of wake velocity on the left side and overestimation on the right side. Note that this three-dimensional wake model is designed to predict the distribution of wake velocity of a single wind turbine without the consideration of wake superposition and mutual interference, therefore, the disparity shown after 6D compared against measurement is acceptable. On the other hand, although the 2DGe model can forecast the wake boundary well in horizontal direction, the values of wake profile were obviously underestimated in all downstream locations from 3D to 8D, especially around the wake center, meaning that the 2DGe model is not capable of predicting the maximal wake deficit. Jensen model still shows poor performance in this case. In addition to the top-hat shape assumption for the wake distribution, the inaccuracy of the Jensen model may attribute to the adopted constant wake expansion rate of 0.075. Although the expansion rate is an empirical value, it is recommended to use a function that includes variables like thrust coefficient and turbulence intensity to describe wake expansion rate as proposed in this paper.

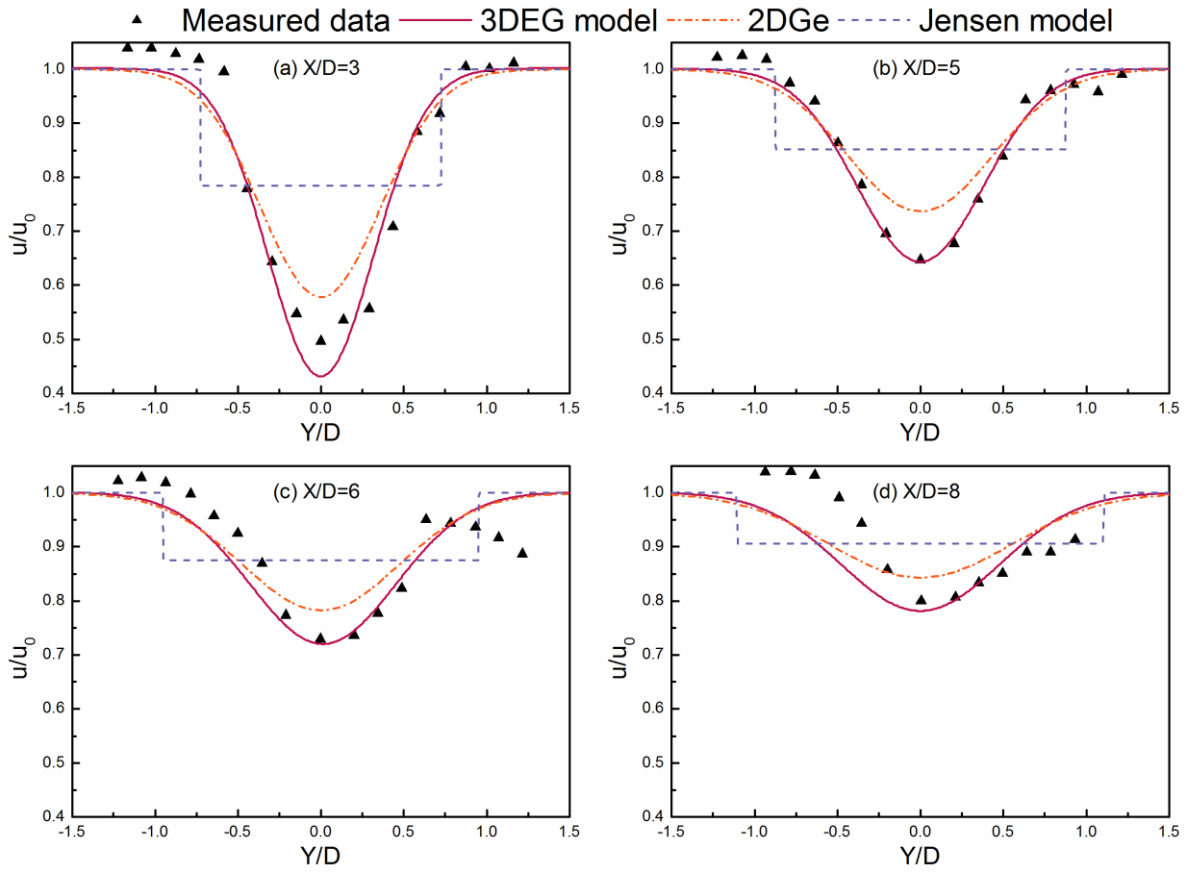

Fig.14 Comparison of horizontal normalized velocity in the wake between the measured data and the predicted results of different wake at three downstream locations.

In order to quantify the discrepancy of prediction shown in Fig. 14, the relative error at each downstream location is calculated. As demonstrated in Table 6, the near wake region has the biggest error, which reaches almost 6.17%. The counterpart from Ge and Jensen has a value of 9.99% and 24.91%, respectively, which seems even less suitable for the near wake region. In the far wake region, the predictive accuracy strongly depends on whether it is influenced by wake interference and superposition effect from adjacent wind turbines. As shown in Fig. 14 and discussed before, measured data at 5D is reliable for error analysis. Wake prediction from 3DEG at 5D has the smallest error among several analytical models with a value of 2.40%, whereas prediction results of the 2DGe model and Jensen model show significant disparity compared with field measurements and therefore cannot be adopted.

The detailed relative errors of each measured data at different downstream locations are presented in Fig. 15. Except for 3D, the proposed 3DEG model works quite well for forecasting the maximal wake deficit as well as wake distribution around the hub center, although an overall trend of underestimation to overestimation from -1.5Y/D to 1.5Y/D can

be found. The figure demonstrates again that the predictive ability of the 5D position that is not affected by the wake superposition is relatively accurate, all the relative errors of which are within ±4%. In addition, at 6D and 8D, the accuracy of prediction is still guaranteed in the area away from the wake boundary that is easily disturbed by adjacent wakes. Therefore, combined with the cases analyzed before, it is reasonable to imagine that wake distribution in the far field beyond 5D would also be well predicted for a single wind turbine.

Table 6 Relative error of the compared models in different downstream distances.

Downstream distance	3D	5D	6D	8D
3DEG relative error	6.17%	2.40%	5.47%	7.25%
2DGe relative error	9.99%	6.01%	6.09%	6.81%
Jensen relative error	24.91%	13.12%	10.82%	8.98%

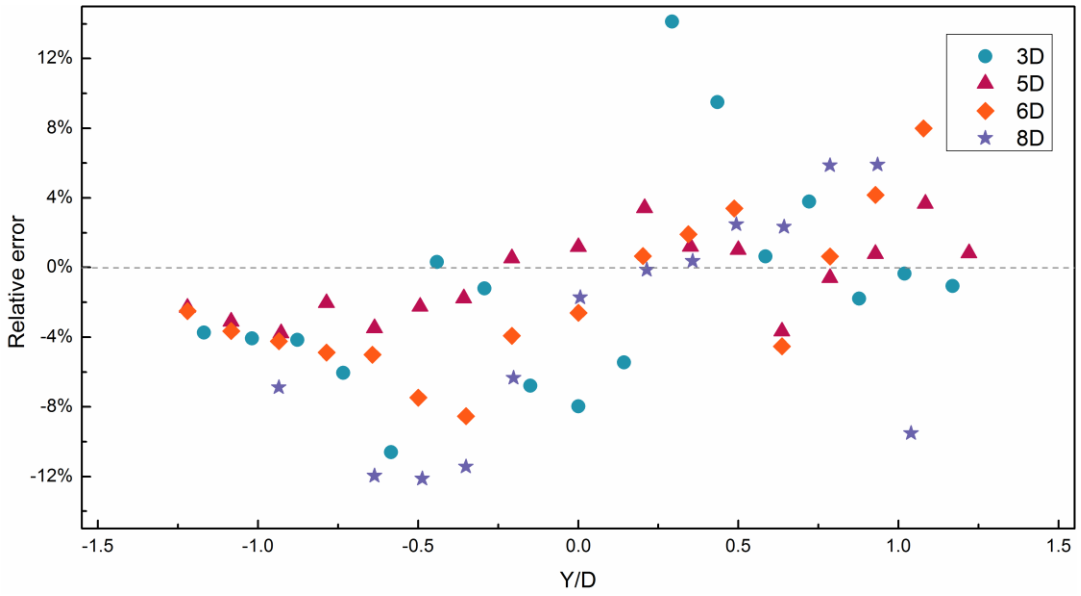

Fig.15 Relative errors in horizontal profiles of the 3DEG model compared against the Shiren Wind Farm measurements.

4.Summary and conclusions

A novel three-dimensional elliptical Gaussian shape wake model is proposed in this paper to help accurately capture the 3D characteristics of the wake profile. Comprehensive validations of the present wake model are conducted by comparing with experimental data

and high-fidelity numerical results for four cases including both miniature and utility-scale wind turbines. The main conclusions are summarized as follows:

(1) A multivariate (instead of axisymmetric) Gaussian distribution is employed in this 3D elliptical Gaussian wake model, which brings the model closer to reality as it truly depends on two independent dimensions (namely horizontal and vertical directions) rather than the radius of a circle. This is due to the fact that turbulence intensity in horizontal direction is larger than that in vertical direction. The most obvious feature corresponding to this is that the proposed model uses different standard deviations for each dimension in the derivation process rather than the same standard deviation. More importantly, for the first time, universal expressions of expansion rate in the horizontal and vertical directions are developed to account for different wake boundaries in each dimension.

(2) Wind shear effect of the inflow is taken into account by using mass conservation law. Due to the wind shear effect, the vertical profiles of velocity in wake show asymmetric distribution rather than a normal distribution, which is resulted from the combination of Gaussian distribution and the wind shear profile. It is found that although the minimum wake velocity near the hub appears slightly below the hub height instead of the exact hub height, the maximal wake deficit does appear at hub height.

(3) Compared with benchmarks, other 3D models are difficult to show their accuracy in all cases, especially the wake deficit around hub height in the near wake region. At the hub height, the 2DGe model is able to predict the wake boundary quite well. However, the maximal wake deficits are apparently underestimated in almost all cases. On the contrary, the accuracy and universality of the proposed wake model are both validated. The proposed 3D elliptical Gaussian wake model is excellent at capturing the characteristics of wake profile in both horizontal and vertical directions in the far-wake region. Its inaccuracy in the near-wake region is due to the ignorance of turbulence variation in height and the far-wake assumption used in mass conservation for its simplicity. In addition, the model is capable of calculating both real-scale wind turbines of different sizes in wind farms and miniature wind turbines in wind tunnels.

(4) The expressions of the model are easy to use and their computational cost is low. The present model can calculate wake velocity at any given downstream spatial position in an accurate and fast manner. No additional numerical calculation or trial calculation is required before this model is applied. Only inflow condition and turbine parameters are required to

calculate the wake distribution of a single wind turbine within a few seconds, which makes it promising for application in wind farms and contributes to wind farm microsite selection and layout optimization.

Declaration of Competing Interest

The authors declare that they have no known competing financial interests or personal relationships that could have appeared to influence the work reported in this paper.

Acknowledgment

The work described in this paper was supported by the Research Institute for Sustainable Urban Development (RISUD) with the account number of BBW8 and the FCE Dean Research project with the account number of ZVHL, The Hong Kong Polytechnic University.

Nomenclature

List of abbreviations

1-D	one-dimensional
2-D	two-dimensional
3-D	three-dimensional
CFD	Computational Fluid Dynamics
D	the rotor diameter of the wind turbine
LES	Large Eddy Simulation
WT	wind turbine

List of symbols

$A(x)$	parameter in 3DEG wake model(m^3/s)
A_0	swept area of the rotor (m^2)
a	axial induction factor
C_T	thrust force coefficient
h_0	hub height of wind turbine (m)
I_0	turbulence intensity
r_0	wind turbine rotor radius (m)
r_1	initial wake radius (m)
r_y	wake-influenced radius in horizontal (Y) direction (m)
r_z	wake-influenced radius in vertical (Z) direction (m)
u_0	inflow wind speed (m/s)
$U(x,y,z)$	wind velocity in 3DEG-U model (m/s)
$U_w(x,y,z)$	wind velocity in 3DEG model (m/s)
k_{Jensen}	wake expansion rate in Jensen model
k_y	wake expansion rate in horizontal (Y) direction
k_z	wake expansion rate in vertical (Z) direction
$S_{elliptical}$	elliptical wake area at any downstream location (m^2)
$\sigma(x)_y$	standard deviation in horizontal (Y) direction (m)
$\sigma(x)_z$	standard deviation in vertical (Z) direction (m)
α	power-law exponent
ρ	air density (kg/m^3)

References

[1] Deng XW, Wu N, Yang K, Chan WL. Integrated design framework of next-generation 85-m wind turbine blade: Modelling, aeroelasticity and optimization. Compos Part B Eng 2019;159:53–61.

[2] Zhou Y, Zheng S, Zhang G. Machine-learning based study on the on-site renewable electrical performance of an optimal hybrid PCMs integrated renewable system with high-level parameters' uncertainties. Renew Energy 2020;151:403–18.

[3] Zhou Y, Cao S, Hensen JLM. An energy paradigm transition framework from negative towards positive district energy sharing networks—Battery cycling aging, advanced battery management strategies, flexible vehicles-to-buildings interactions, uncertainty and sensitivity analysis. Appl Energy 2021;288:116606.

[4] Chen J, Lu L. Comprehensive evaluation of thermal and energy performance of radiative roof cooling in buildings. J Build Eng 2021;33:101631.

[5] Shakoor R, Hassan MY, Raheem A, Wu YK. Wake effect modeling: A review of wind farm layout optimization using Jensen's model. Renew Sustain Energy Rev 2016;58:1048–59. https://doi.org/10.1016/j.rser.2015.12.229.

[6] Lee J, Zhao F, Dutton A, Backwell B, Fiestas R, Qiao L, et al. Global wind report 2019. Brussels Glob Wind Energy Counc 2020.

[7] Barthelmie RJ, Hansen K, Frandsen ST, Rathmann O, Schepers JG, Schlez W, et al. Modelling and measuring flow and wind turbine wakes in large wind farms offshore. Wind Energy An Int J Prog Appl Wind Power Convers Technol 2009;12:431–44.

[8] Ti Z, Deng XW, Yang H. Wake modeling of wind turbines using machine learning. Appl Energy 2020;257:114025. https://doi.org/10.1016/j.apenergy.2019.114025.

[9] Wu YT, Porté-Agel F. Large-Eddy Simulation of Wind-Turbine Wakes: Evaluation of Turbine Parametrisations. Boundary-Layer Meteorol 2011;138:345–66. https://doi.org/10.1007/s10546-010-9569-x.

[10] Sun H, Qiu C, Lu L, Gao X, Chen J, Yang H. Wind turbine power modelling and optimization using artificial neural network with wind field experimental data. Appl Energy 2020;280:115880. https://doi.org/10.1016/j.apenergy.2020.115880.

[11] Sun H, Gao X, Yang H. A review of full-scale wind-field measurements of the wind-turbine wake effect and a measurement of the wake-interaction effect. Renew Sustain Energy Rev 2020;132:110042. https://doi.org/10.1016/j.rser.2020.110042.

[12] Jensen NO. A note on wind generator interaction 1983.

[13] Katic I, Højstrup J, Jensen NO. A simple model for cluster efficiency. Eur. Wind energy Assoc. Conf. Exhib., vol. 1, 1986, p. 407–10.

[14] Archer CL, Vasel-Be-Hagh A, Yan C, Wu S, Pan Y, Brodie JF, et al. Review and evaluation of wake loss models for wind energy applications. Appl Energy 2018;226:1187–207. https://doi.org/10.1016/j.apenergy.2018.05.085.

[15] Frandsen S, Barthelmie R, Pryor S, Rathmann O, Larsen S, Højstrup J, et al. Analytical modelling of wind speed deficit in large offshore wind farms. Wind Energy An Int J Prog Appl Wind Power Convers Technol 2006;9:39–53.

[16] Schlichting H, Gersten K. Boundary-layer theory. Springer; 2016.

[17] Shengbai Xie. Self-similarity and turbulence characteristics of wind turbine wakes via large-eddy simulation. Wind Energy 2013:1–20. https://doi.org/10.1002/we.

[18] Sun H, Gao X, Yang H. Experimental study on wind speeds in a complex-terrain wind farm and analysis of wake effects. Appl Energy 2020;272:115215. https://doi.org/10.1016/j.apenergy.2020.115215.

[19] Sun H, Gao X, Yang H. Validations of three-dimensional wake models with the wind field measurements in complex terrain. Energy 2019;189:116213. https://doi.org/10.1016/j.energy.2019.116213.

[20] Gao X, Yang H, Lu L. Optimization of wind turbine layout position in a wind farm using a newly-developed two-dimensional wake model. Appl Energy 2016;174:192–200. https://doi.org/10.1016/j.apenergy.2016.04.098.

[21] Ge M, Wu Y, Liu Y, Li Q. A two-dimensional model based on the expansion of physical wake boundary for wind-turbine wakes. Appl Energy 2019;233–234:975–84. https://doi.org/10.1016/j.apenergy.2018.10.110.

[22] Ge M, Wu Y, Liu Y, Yang XIA. A two-dimensional Jensen model with a Gaussian-shaped velocity deficit. Renew Energy 2019;141:46–56.

https://doi.org/10.1016/j.renene.2019.03.127.

[23] Bastankhah M, Porté-Agel F. A new analytical model for wind-turbine wakes. Renew Energy 2014;70:116–23. https://doi.org/10.1016/j.renene.2014.01.002.

[24] Dou B, Guala M, Lei L, Zeng P. Wake model for horizontal-axis wind and hydrokinetic turbines in yawed conditions. Appl Energy 2019;242:1383–95. https://doi.org/10.1016/j.apenergy.2019.03.164.

[25] Brogna R, Feng J, Sørensen JN, Shen WZ, Porté-Agel F. A new wake model and comparison of eight algorithms for layout optimization of wind farms in complex terrain. Appl Energy 2020;259:114189. https://doi.org/10.1016/j.apenergy.2019.114189.

[26] Sun H, Yang H. Study on an innovative three-dimensional wind turbine wake model. Appl Energy 2018;226:483–93. https://doi.org/10.1016/j.apenergy.2018.06.027.

[27] Sun H, Yang H. Numerical investigation of the average wind speed of a single wind turbine and development of a novel three-dimensional multiple wind turbine wake model. Renew Energy 2020;147:192–203. https://doi.org/10.1016/j.renene.2019.08.122.

[28] Ishihara T, Qian GW. A new Gaussian-based analytical wake model for wind turbines considering ambient turbulence intensities and thrust coefficient effects. J Wind Eng Ind Aerodyn 2018;177:275–92. https://doi.org/10.1016/j.jweia.2018.04.010.

[29] Dou B, Qu T, Lei L, Zeng P. Optimization of wind turbine yaw angles in a wind farm using a three-dimensional yawed wake model. Energy 2020;209:118415. https://doi.org/10.1016/j.energy.2020.118415.

[30] Abkar M, Porté-Agel F. Influence of atmospheric stability on wind-turbine wakes: A large-eddy simulation study. Phys Fluids 2015;27. https://doi.org/10.1063/1.4913695.

[31] Gao X, Li B, Wang T, Sun H, Yang H, Li Y, et al. Investigation and validation of 3D wake model for horizontal-axis wind turbines based on filed measurements. Appl Energy 2020;260. https://doi.org/10.1016/j.apenergy.2019.114272.

[32] Tennekes H, Lumley JL. A First Course in Turbulence. 1972. https://doi.org/10.7551/mitpress/3014.001.0001.

[33] Burton T, Sharpe D, Jenkins N, Bossanyi E. Wind energy handbook. vol. 2. Wiley

Online Library; 2001.

[34] Jensen NO. A note on wind generator interaction. Risø-M-2411 Risø Natl Lab Roskilde 1983:1–16.

[35] Barthelmie RJ, Larsen GC, Frandsen ST, Folkerts L, Rados K, Pryor SC, et al. Comparison of wake model simulations with offshore wind turbine wake profiles measured by sodar. J Atmos Ocean Technol 2006;23:888–901.

[36] Barthelmie RJ, Frandsen ST, Nielsen MN, Pryor SC, Rethore P, Jørgensen HE. Modelling and measurements of power losses and turbulence intensity in wind turbine wakes at Middelgrunden offshore wind farm. Wind Energy An Int J Prog Appl Wind Power Convers Technol 2007;10:517–28.

[37] Akay B, Ragni D, Ferreira CS, Bussel GJW Van. Investigation of the root flow in a Horizontal Axis. Wind Energy 2013:1–20. https://doi.org/10.1002/we.

[38] Wind T, Design F. GH WindFarmer 2006:0–16.